Case Studies in Nondestructive Testing and Evaluation 6 (2016) 45–52

Contents lists available at ScienceDirect

Case Studies in Nondestructive Testing and Evaluation

www.elsevier.com/locate/csndt

High resolution pore size analysis in metallic powders by X-ray tomography

K. Heim [a,*,1], F. Bernier [b], R. Pelletier [b], L.-P. Lefebvre [b]

[a] Technische Universität Berlin, Hardenbergstraße 36, 10623 Berlin, Germany
[b] National Research Council Canada, 75, Boulevard de Mortagne, Boucherville, QC, J4B 6Y4, Canada

ARTICLE INFO

Article history:
Available online 3 October 2016

ABSTRACT

The deployment of additive manufacturing processes relies on part quality, specifically the absence of internal defects. Some of those defects have been associated with porosities in the powder feedstock. Since the level of porosity in the powder is generally very low, standard characterisation techniques such as pycnometry and metallography are not suitable for quantification. However, the quantification of such micro sized porosity in metallic powders is crucial to better understand the potential source of internal defects in final components and for quality control purposes. X-ray tomography with a 3 µm resolution offers the possibility to visualise pores in large volume of powder and to quantify their geometrical features and volume fraction using image analysis routines. This combination is unique and demonstrates the power of the approach in comparison to standard powder characterisation techniques. Results presented show the prospects and limits of this technique depending on the imaging device, material and image analysis procedure.

© 2016 Published by Elsevier Ltd. This is an open access article under the CC BY-NC-ND license (http://creativecommons.org/licenses/by-nc-nd/4.0/).

1. Introduction

Additive Manufacturing (AM) describes a family of processes to build objects layer by layer [1–3]. Those techniques offer the capability of manufacturing efficiently components with topographically optimised geometries, directly from computer aided designs without extensive machining. However, establishing large scale AM processes relies on part quality, especially the absence of internal defects and part-to-part consistency [4]. Absence of defects is also crucial for other types of powder metallurgy processes [5].

Some of the defects observed in finished parts produced using AM processes including powder bed, laser cladding, and cold spray have been associated with porosities in the powder feedstock. Given the very low level of porosity generally observed in those powders, standard characterisation techniques such as pycnometry and metallography with image analysis are not suitable for quantification [6–8]. Metallography does not allow adequate statistical characterisation of 3D features. In one study, the particle-pore-ratio was quantified by analysing 40–70 particles sample which contained 10–20 contained pores [9]. With such small samples, porosity evaluation can be adequate only when a high fraction of the particles is porous. When a very small fraction of the particles contains pores, the sample size required for the analysis to be statistically significant becomes impractical. Pycnometry, on the other hand, allows studying a great number of particles but does not provide

* Corresponding author.
E-mail address: korbinian.heim@helmholtz-berlin.de (K. Heim).
[1] Fax: +4930806243059.

http://dx.doi.org/10.1016/j.csndt.2016.09.002
2214-6571/© 2016 Published by Elsevier Ltd. This is an open access article under the CC BY-NC-ND license (http://creativecommons.org/licenses/by-nc-nd/4.0/).

a pore size distribution and cannot be used with a high level of confidence on alloys due to the uncertainty associated with the theoretical density of the material. Indeed, the range in alloy theoretical density as defined by specifications (i.e. associated with interval of compositions) can introduce variations equivalent to the cumulative volume of internal pores, therefore prohibiting accurate quantification of porosity levels.

X-ray-CT (XCT) combined with 3D image analysis has been used to study packing of aspherical particles (notably the random close packing transition [10–12]). XCT was also used to evaluate the porosity in steel [13], Ti6Al4V [14] and CoCrMo [15] samples produced by selective laser melting (SLM) [13,15] or selective electron beam melting (SEBM) [14]. Investigating the inner porosity of the initial particle feedstock is in comparison much more complex as three phases have to be separated: the particles, the intermediate phase between the particles and the gaseous phase inside the particles – namely pores. Evaluating and quantifying the level of porosity in particles using MicroCT and 3D image analysis in Ti–6Al–4V powder (mean powder size of 40–100 µm) was first presented by Tammas-Williams et al. [14]. They concentrated their work mainly on the pore quantification contained in a component manufactured by SEBM, but they also investigated the porosity of the powder feedstock. The volume they analysed was 2.7 mm^3 and they detected 970 pores having a median diameter of 12.1 µm. However, no data was provided on the reliability of pore size detection and on the image analysis routine.

The present paper offers a detailed evaluation of particle porosity in various metals. The image analysis routine as well as the sizes, shapes and pore fraction obtained with the method is presented. Results are compared with those obtained with pycnometry and image analysis on 2D metallographic sections.

2. Experimental

Two types of pure titanium powders with different atomisation technique (plasma atomisation from AP&C with a $D_{50} =$ 76 µm and gas atomisation from TLS with a $D_{50} = 98$ µm), a pure aluminium (gas atomisation from Valimet) and a pure magnesium powder (gas atomisation from Magnesium Elektron) were used to test the ability of the image analysis routine to quantify the particle porosity.

To scan the powders using a MicroCT, cylindrical specimens of the different powders were embedded in an epoxy resin and machined into rods of 3.175 mm (1/8″) in diameter to obtain a fixed volume and to be as close as possible to the X-ray source to achieve maximal magnification (about 65×). Radioscopies were acquired using a Nikon HMXST 225 computed tomography system with a minimal focal spot size of 3 µm and a Perkin–Elmer 1621 AN amorphous silicon flat panel (409.6 × 409.6 mm) coupled with a CsI scintillator. The X-ray source was operated at 135 kV and 64 µA with a 0.5 mm Cu filter to reduce beam hardening. The typical voxel size was 3 µm for all powders, except the Mg powder where a 3.8 µm voxel size was used. To build the 3D XCT images, 3142 radioscopies (i.e. projections) with an exposure time of 1000 ms and 8 integrated frames were acquired and reconstructed using the internal Nikon software. The subsequent image analysis was performed using the ImageJ software.

The powder porosity was measured using a Helium gas pycnometer from Micromeritics and calculated using the difference between the measured density and the theoretical density of the metal. Metallographic observations were also conducted on as-polished samples at a magnification of 200× using a Clemex Vision image analysis system to validate the results.

3. Image analysis routine

Pores of the powder feedstock were detected, separated and quantified using an image analysis routine written in ImageJ. The procedure, as drawn in Fig. 1, begins with several user interactions to crop and scale the original raw image, Fig. 1(a). Five different Median filters were applied to find the best compromise between noise reduction and blurring of the images. Different levels of Gaussian filter were then used to reduce contrast deviation between particles, resin and pores and find the best compromise to completely select the particle volume, without merging the particles. The background (resin and pores) is thereby separated from the particles. The decisions on the Median and the Gaussian filter were taken by the user as the human eye is the best indicator.

The following steps were executed on a reduced image sequence to save computational time. Fig. 1(a), as well as all images explaining the image analysis routine, show a reduced field of view (FOV) of the titanium sample (median diameter $D_{50} = 76$ µm). For the 3D filters, the plugins Fill Holes 3D, Distance Map, Local Maxima, Watershed Transformation and 3D Geometrical Measurement were executed using the 3D ImageJ Suite [16]. For the Sphericity filter, the plugin Xlib based on reference [17] was used. One challenge during the preparation of the image analysis routine was to adapt the method to characterise several materials of various densities (contrasts), different pore and particle sizes, shapes, distributions and pore-particle-ratios, see Fig. 2.

Once the best filters are found to correct the original image, using the procedure in Fig. 1, those values are used to correct the entire stack (filter and background correction by subtraction) to get cleaner and optimised images. Afterwards, the correction procedure presented in Fig. 3 is used to separate the pores. Four different threshold-based segmentation algorithms are used (b–e) to detect as most and different kind of pores as possible. (f–i) [18–20]. “0,0” in (d) means that all dark values (resin/pores) after background correction are kept. The first two algorithms (b, c) deal with separated particles (thresholding the white areas to 1), whereby those porous particles (white) are filled in 3D using a ImageJ plugin leading to separated pores (black) by subtracting the image with and without filled pores (f, g). The other two procedures (d, e) address the gaseous phase (thresholding the dark areas to 1), after which two segmentation algorithms are used to

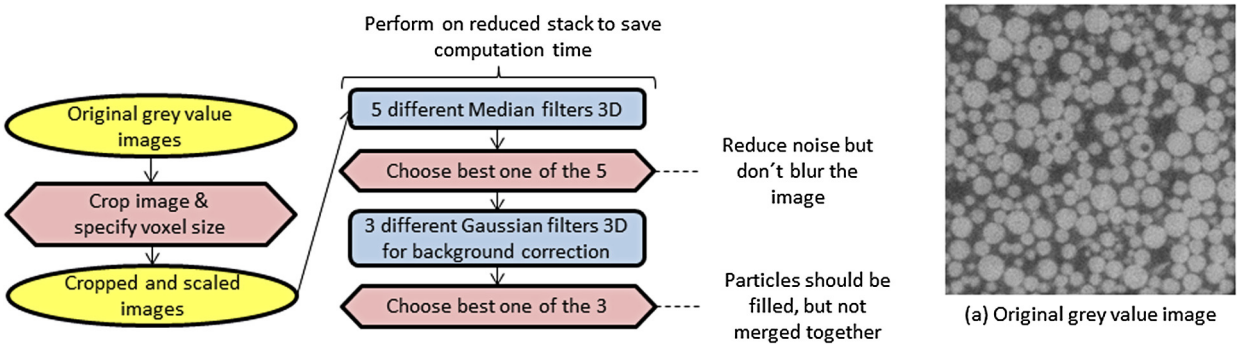

Fig. 1. Flow chart of the image correction procedure used to improve the quality of the raw image (a). Red boxes indicate active interactions with user.

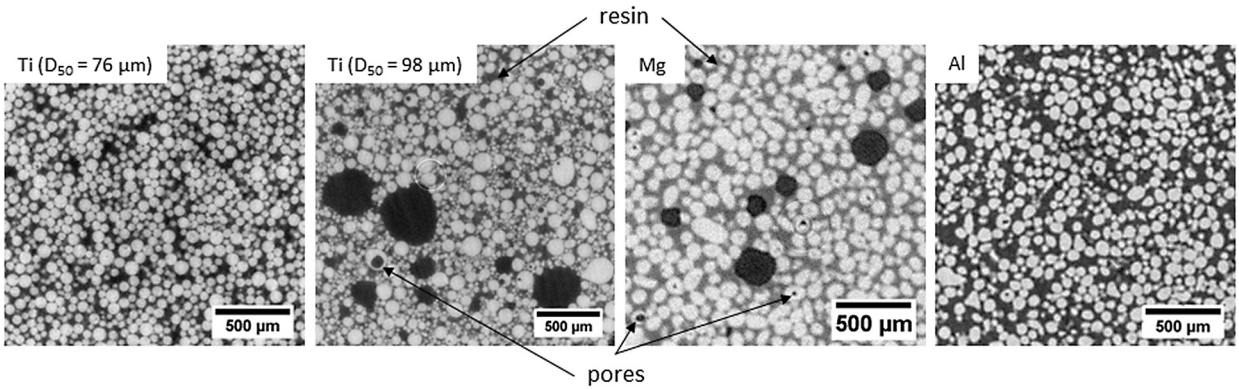

Fig. 2. Reconstructed slices (unprocessed) acquired with the MicroCT of four different materials. Particles are white resin is grey and pores are black.

highlight different kind of pores (almost open pores I and II). Both procedures separate the pores using the Sphericity filter, as the pores inside particles exhibit a spherical morphology while interstice between particles are not spherical [17]. It has to be mentioned that images in (e) and (i) are taken from another area of the sample as no results are found in the original FOV. The 3D erosion process under (d) is used to separate partially connected pores from the surrounding resin (caused by limited resolution and noise) and the change in size is compensated after sphericity filtering by dilation. For this purpose, the ImageJ 3D Toolkit Plugin is used [21]. As some small artificial pores caused by the noise in the images cannot be avoided, a small Median or Opening filter (1 px, respectively $3 \times 3 \times 3$ vxl) is subsequently applied to remove these artefacts. Eventually, to avoid any duplication of detected pores, all images are binary merged together. The accuracy of the image processing and pore detection can be visualised and confirmed by the user before continuing the quantification of the results, see Fig. 4.

Once the pore separation is considered successful, the volume of the particles can be measured to evaluate the pore-particle ratio. The user can then decide if the pore-particle volume ratio should be expressed by volume, by count or both. If only the volume ratio is required, computation time can be saved, as particles do not have to be separated and the entire volume of particles can be quantified by simple thresholding (using the Minimum algorithm), see Fig. 5. Fig. 5(j) shows the accumulation of all pores along one axis in a 3D image. The corresponding cumulative pore size distribution is shown in Fig. 5(k).

4. Results

Comparing the images of extracted pores and particles with the raw images suggests that the developed image analysis routine and quality of images provided by the MicroCT was adequate for all the tested materials. Fig. 6 presents the four pore-size distributions obtained with the powders analysed.

The obtained number of pores, particles and pore/particle ratio can be seen in Table 1. It has to be mentioned that the total volume investigated varied slightly. It was found that all materials show a reliable amount of pores and a relatively high pore-particle ratio. The results indicate that quantitative data on the size of the pores can be obtained. Indeed, the pore-particle ratios were significantly different from powder to powder, Ti ($D_{50} = 76$ µm) having pores $2\times$ smaller than the Ti ($D_{50} = 98$ µm) powder and $4.5\times$ smaller than the Mg powder (relative to the particle volume).

The influence of the different segmentation algorithms was studied only for the Ti ($D_{50} = 76$ µm) powder on a reduced image stack and the results are presented in Table 2. By comparing the results between the volume and number %, it is clear that 'Isodata' detect mostly small pores while '0,0' will detect the largest pores. "Isodata" was found to be the most

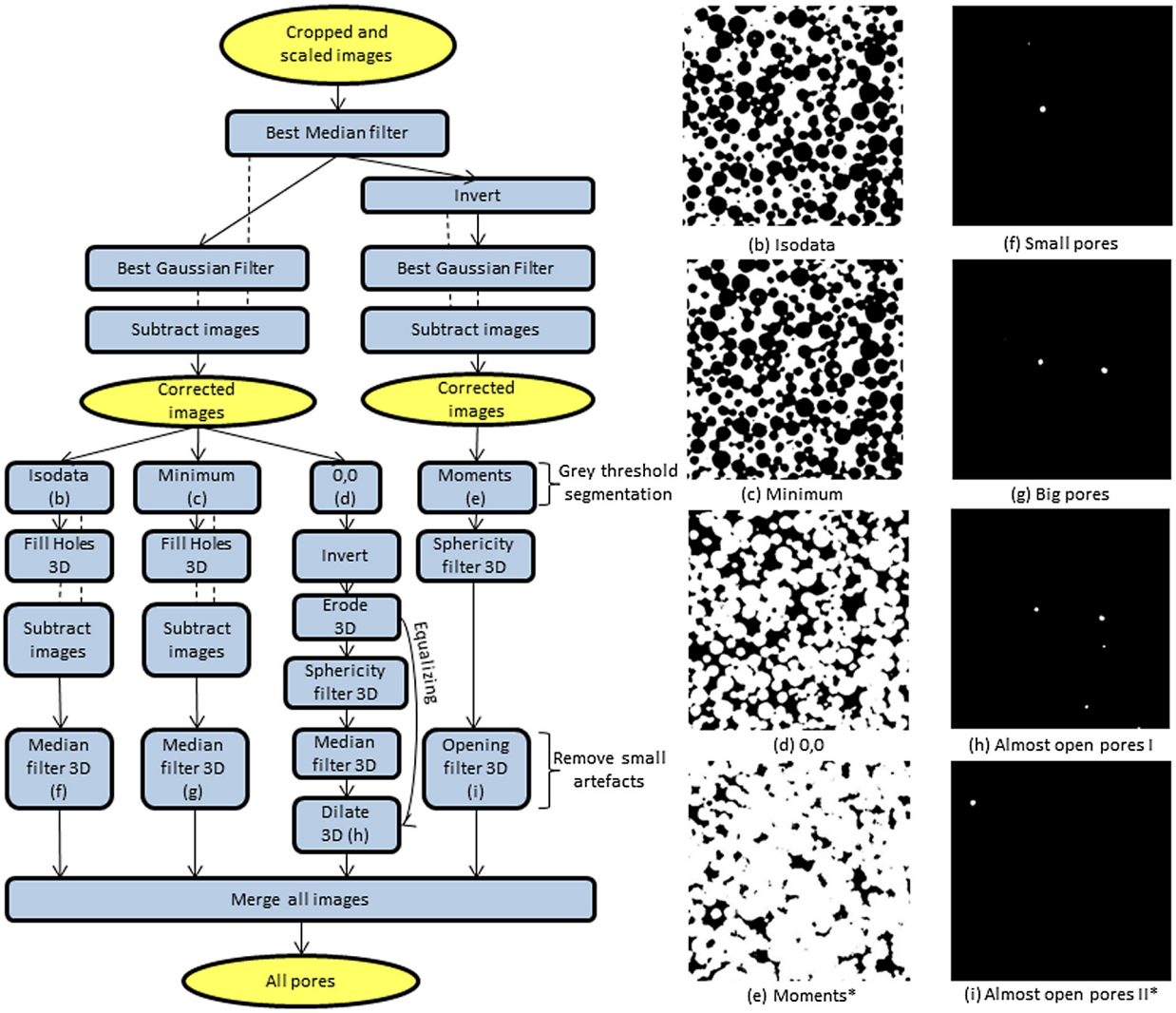

Fig. 3. Flow chart of the pore extraction routine. The first step is to apply the selected filtering values to the entire stack of images (see Fig. 1). The grey thresholding algorithms are shown on the left in (b)–(d), the resulting separated pores are shown on the right in (f)–(i). Procedures (b) and (c) deal with the particles, while (d) and (e) address the gaseous phase. *The images (e) and (i) show a different area of the sample as no effect can be seen in the first FOV. The dashed lines represent the two images which are subtracted.

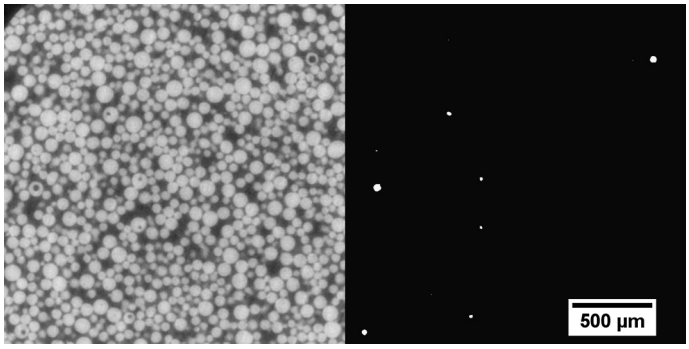

Fig. 4. The corrected, cropped and scaled grey image (left) is shown in comparison to the binarized extracted pore image (right).

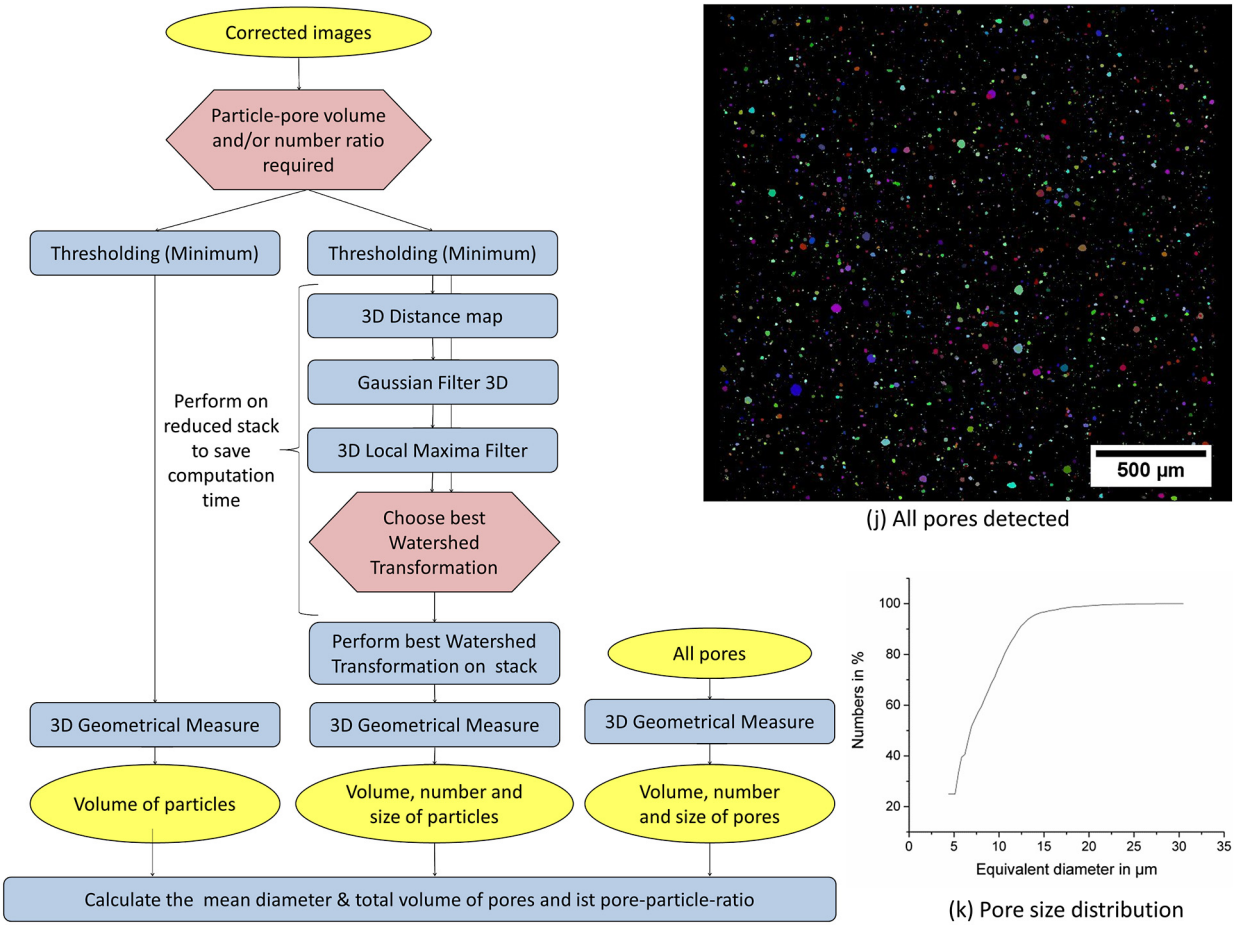

Fig. 5. Flow chart of the particle analysis routine. It starts with the same corrected stack of images as in Fig. 3. This routine analyses the particles (volume and/or number) to calculate the mean diameter, the total volume of pores and the pore-particle ratio (volume and/or number). An example of extracted pores contained in a titanium powder ($D_{50} = 76$ µm) obtained from a stack of 1440 images (slices) is shown in (j). In (k) the resulting pore size distribution is presented.

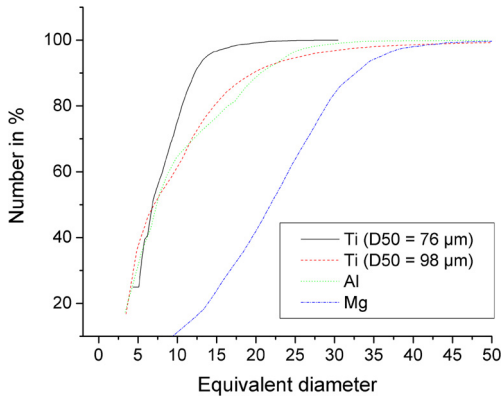

Fig. 6. Pore size distribution of various metallic powder feedstocks.

powerful algorithm detecting most of the pores in regard of pore volume and number. When merging the results from all the algorithms ("All"), 33.9 vol.% and 19.5 num.% of detected pores was eliminated due to overlapping volume (i.e. pores counted by different algorithm).

In Table 3, the mean porosity values obtained using MicroCT are compared to standard characterisation methods: pycnometry and metallography. The given porosity variance of pycnometry is caused by different theoretical density values

Table 1
Number of pores, particles and pore/particle ratio analysed for tested metal powders.

Sample	Number of pores	Number of particles	Pore-particle ratio (vol.%)
Ti ($D_{50} = 76$ µm)	2444	32785	7.5
Ti ($D_{50} = 98$ µm)	8658	54316	15.9
Al	2016	20888	9.7
Mg	2428	7205	33.7

Table 2
Influence of the segmentation algorithms on the porosity detected.

	Isodata	0,0	Minimum	Moments	All
Porosity in vol.%	0.044	0.027	0.027	0.015	0.075
Weighted vol.%	38.7	24.0	24.0	13.3	
Weighted num.%	58.9	5.9	32.8	2.4	

Table 3
Porosity values obtained from MicroCT, pycnometry and metallography for various materials.

Sample	MicroCT in vol.%	Pycnometry in vol.%	Metallography in area %
Ti ($D_{50} = 76$ µm)	0.051	0.022–0.17	0.078
Ti ($D_{50} = 98$ µm)	0.424	0.31–0.47	0.68
Al	0.129	0–0.16	–
Mg	0.73	0.29–0.40	–

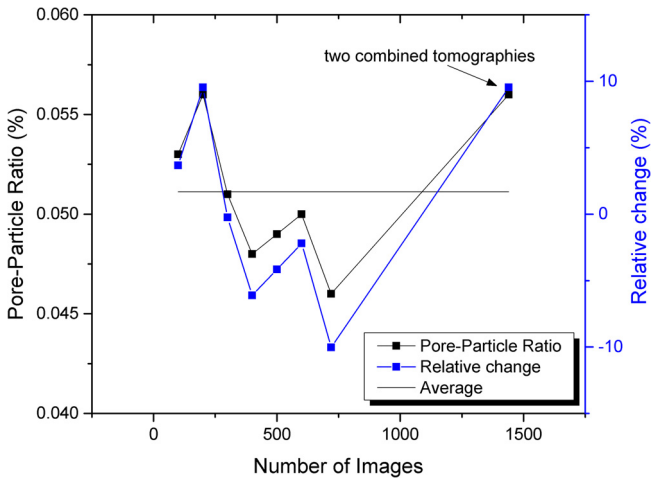

Fig. 7. Porosity depending on the number of images used and its change relative to the average value.

used [22–25]. It is shown that except for magnesium, all porosity values obtained by MicroCT are in the range of those obtained by pycnometry.

Regarding metallography on polished cross sections, only titanium powders were investigated using image analysis on 75 images each. The porosity values are a bit larger (1.5–1.6×) than the values measured by MicroCT and within the range of pycnometry for the $D_{50} = 76$ µm powder, but not for the $D_{50} = 98$ µm powder. The results obtained allow to discriminate the amount of porosity in the powders. For example, the porosity content evaluated in the Ti ($D_{50} = 98$ µm vs Ti ($D_{50} = 76$ µm)) is significantly larger (∼8× when comparing the MicroCT and metallography) and consistent with the pycnometry measurements while the amount of porosity in the Mg powder is 14× the amount in the Ti ($D_{50} = 76$ µm) powder.

To evaluate the reliability of the MicroCT as a function of the number of images (i.e. slices), the porosity was measured using stacks containing different number of images. The thickness of one image slice corresponds to the voxel size used. Fig. 7 shows the variation of calculated porosity depending on the number of images used in a stack. It can be seen that the calculated porosity fluctuates as the number of slices increases. The relative change of porosity is always within 10% of the value obtained with the entire stack; which indicates the reliability of the image analysis routine using MicroCT. Moreover, such a variation is expected to be caused by natural variation within the sample; as supported by the visual inspection of the image slices. In contrast, the uncertainty associated with the theoretical density and the variation in the final measured density caused fluctuations up to 56% in the pycnometry values.

5. Discussion

The presented image analysis routine was found to work well for the evaluation of porosities, pore and particle sizes, shapes and distributions in powder of different materials, see Fig. 2 and compare results in Fig. 6 and Table 3. However, the main issue of evaluating the accuracy and reliability of this new method remains, as no accurate reference method exists. To minimise possible misinterpretation, MicroCT results were first checked visually, like in Fig. 4, and were subsequently compared to pycnometry and metallography results. Doing so, it was found that all results are of the same order of magnitude and even coincide in most of the cases (see Table 3).

When MicroCT and standard characterisation methods results are compared, it can be noted that pycnometry has the advantage to characterise larger volume of particles than X-ray computed tomography (single scan). However, porosities calculated using densities obtained by pycnometry are highly sensitive to the theoretical density value used and to the variation in the measured density itself [22–25]. Moreover, pycnometry is limited to very pure metals or materials with density known with high precision as density variations in common alloys is by far bigger than the porosity values observed in high quality powders. Metallographic analysis has the highest spatial resolution of all the standard techniques. MicroCT is of course limited by the smallest achievable voxel size, whereas metallography can be used to visualise pores in the sub-µm range. The 3 µm voxel size is the minimal voxel size achievable with the MicroCT used is this study. In a previous paper and for the same type of powder, it was shown that the maximum voxel size to get reasonable data on the particle size was 5 µm, which is, however, not sufficient to quantify reliably the porosity of the powder [26]. On the other hand, metallography only generates 2D data, wherefore pore dimensions can only be calculated by multiplying the measured 2D values with constants to obtain the equivalent spherical diameter [27]. Some small pores identified as individual might also be connected, leading to misinterpretation. The small number of pores analysed, ∼200 in comparison to ∼5000 for MicroCT, is another general statistical source of error. This fact seems, however, to play only a secondary effect as Fig. 7 shows that even a small number of MicroCT images lead to a pretty good approximation of the average porosity value.

MicroCT and the developed image analysis routine is the only method allowing the quantification of 3D information, like those presented in Table 1 and Table 3. Table 2, collected from a relatively large number of particles. Even though the evaluation of porosity is not perfect due to limited spatial resolution, resulting in missing pores or imperfect separation of pores and matrix, porosity values obtained are in the same range as the one measured with known standard characterisation methods proving its practicality. The differences observed seems to be significant reliable and allow to differentiate the porosity (amount and size) in different powders. All segmentation algorithms used were found to be required, even though the number of pores detected by “0,0” and “Moments” seems to be negligible, their impact on the volume percentage is noteworthy, compare Table 2. Thus it can be concluded that “Isodata” and “Minimum” are required to find most of the pores (small but many), whereas “0,0” and “Moments” are required to detect the fewer but bigger pores. Additional information like the pore-particle ratio (in number or volume) or pore-size distribution can also be obtained with the technique. As the developed image analysis routine is automatised, it is less susceptible to user-to-user variance whereby leading to more comparable results. The procedure could be further validated using experimental set-up with better resolution and signal/noise ratio. The impact of the micro-pores observed (in the powder) on the final material properties and product performance remains questionable and also needs to be further investigated.

6. Summary

- The porosity of various metallic powder feedstocks was successfully quantified using a MicroCT device and an image analysis routine.
- Determined porosity values analysed are comparable to the results obtained by standard characterisation methods (pycnometry, image analysis on metallographic 2D sections).
- The automated image analysis routine is applicable for various materials investigated in this study having different densities (contrasts), pore and particle sizes, shapes, distributions and pore-particle ratios.
- MicroCT is found to be the only method capable of quantifying 3D information on a large number of particles.
- Results obtained should be reliable to compare the porosity (amount and size) in different types of powders.

References

[1] Gibson I, Rosen DW, Stucker B. Additive manufacturing technologies. Springer; 2010.
[2] Campbell I, Bourell D, Gibson I. Additive manufacturing: rapid prototyping comes of age. Rapid Prototyping J 2012;18:255–8.
[3] Kruth J-P, Leu MC, Nakagawa T. Progress in additive manufacturing and rapid prototyping. CIRP Ann 1998;47:525–40.
[4] du Plessis A, le Roux SG, Els J, Booysen G, Blaine DC. Application of microCT to the non-destructive testing of an additive manufactured titanium component. Case Stud Nondestruct Test Eval 2015;4:1–7.
[5] Lame O, Bellet D, Di Michiel M, Bouvard D. Bulk observation of metal powder sintering by X-ray synchrotron microtomography. Acta Mater 2004;52:977–84.
[6] Thijs L, Verhaeghe F, Craeghs T, Van Humbeeck J, Kruth J-P. A study of the microstructural evolution during selective laser melting of Ti–6Al–4V. Acta Mater 2010;58:3303–12.
[7] Parthasarathy J, Starly B, Raman S. A design for the additive manufacture of functionally graded porous structures with tailored mechanical properties for biomedical applications. J Manuf Process 2011;13:160–70.
[8] Karlsson J, Snis A, Engqvist H, Lausmaa J. Characterization and comparison of materials produced by Electron Beam Melting (EBM) of two different Ti–6Al–4V powder fractions. J Mater Process Technol 2013;213:2109–18.

[9] Huron ES, Casey RL, Henry MF, Mourer DP. In: Kissinger ID, Deye DJ, Anton DL, Cerel AD, Nathal MV, Pollock TM, et al., editors. Superalloys. The Minerals, Metals & Materials Society; 1996.
[10] Schaller FM, et al. Tomographic analysis of jammed ellipsoid packings. AIP Conf Proc 2013;1542:377–80.
[11] Aste T, Saadatfar M, Senden TJ. Geometrical structure of disordered sphere packings. Phys Rev E 2005;71:61302.
[12] Athanassiadis AG, et al. Particle shape effects on the stress response of granular packings. Soft Matter 2014;10:48–59.
[13] Ziółkowski G, Chlebus E, Szymczyk P, Kurzac J. Application of X-ray CT method for discontinuity and porosity detection in 316L stainless steel parts produced with SLM technology. Arch Civ Mech Eng 2014;14:608–14.
[14] Tammas-Williams S, et al. XCT analysis of the influence of melt strategies on defect population in Ti–6Al–4V components manufactured by selective electron beam melting. Mater Charact 2015;102:47–61.
[15] Monroy K, Delgado J, Ciurana J. Study of the pore formation on CoCrMo alloys by selective laser melting manufacturing process. Proc Eng 2013;63:361–9.
[16] Ollion J, Cochennec J, Loll F, Escudé C, Boudier T. TANGO: a generic tool for high-throughput 3D image analysis for studying nuclear organization. Bioinformatics 2013;29:1840–1.
[17] Wadell H. Volume shape and roundness of quartz particles. J Geol 1935;43:250–80.
[18] Ridler T, Calvard S. Picture thresholding using an iterative selection method. IEEE Trans Syst Man Cybern 1987;8:630–2.
[19] Prewitt J, Mendelsohn M. The analysis of cell images. Ann NY Acad Sci 1996;128:1035–53.
[20] Tsai W. Moment-preserving thresholding: a new approach. Comput Vis Graph Image Process 1985;29:377–93.
[21] IJ Plugins Toolkit. Available from: http://ij-plugins.sourceforge.net/index.html [accessed 26 April 2016].
[22] James AM, Lord MP. Macmillan's chemical and physical data. 1992.
[23] Lide DR. Chemical Rubber Company handbook of chemistry and physics. CRC Press; 1996.
[24] Dean JA. Lange's handbook of chemistry. McGraw–Hill; 1992.
[25] MatWeb. Available from: http://www.matweb.com/index.aspx [accessed 5 October 2016].
[26] Bernier F, Pelletier R, Lefebvre L-P, Heim K. Powder characterization using X-ray tomography and image analysis. Adv Powder Metall Part Mat 2016:1–10. http://nparc.cisti-icist.nrc-cnrc.gc.ca/eng/view/object/?id=485f564f-02ba-4ff8-81fb-8ff44941c4d2. NPARC number: 23000757 Record identifier: 485f564f-02ba-4ff8-81fb-8ff44941c4d2.
[27] Jennings BR, Parslow K. Particle size measurement: the equivalent spherical diameter. R Soc Lond Proc, Ser A, Math Phys Eng Sci 1988;419:137–49.